JOURNAL OF GEOPHYSICAL RESEARCH, VOL. 104, NO. D10, PAGES 12,177–12,191, MAY 27, 1999

Sensitivity of the simulated Asian summer monsoon to parameterized physical processes

Zachary A. Eitzen and David A. Randall
Department of Atmospheric Science, Colorado State University, Fort Collins

Abstract. A study of the sensitivity of the simulated Asian summer monsoon to changes in general circulation model formulation is reported. The baseline version of the model fails to realistically simulate the precipitation, wind, and temperature fields. In one experiment the stratiform cloud parameterization was changed from a simple large-scale saturation scheme to a scheme that prognostically determines cloud water, cloud ice, and rain. In a second experiment a parameter that relates the cumulus mass flux to the cumulus kinetic energy was altered so as to increase the convective adjustment time. These changes in the stratiform and cumuliform cloud parameterizations significantly improve the simulations of the precipitation and upper level wind fields, respectively.

1. Introduction

According to *Webster* [1987] a monsoon can be regarded as a longitudinally localized Hadley circulation. Monsoons are strongly influenced by such diabatic processes as the absorption of solar radiation by the lower boundary, the regulation of the surface sensible and latent heat fluxes by land-surface processes, and the release of latent heat in convective and stratiform clouds. The circulation of the Asian summer monsoon, in particular, is enhanced by surface heating of the Tibetan Plateau, which towers above the surrounding land surface.

After the seasonal snow has melted, the surface albedo of the plateau region decreases, and the increased absorption of solar radiation warms the surface of the plateau and the air above it relative to the surrounding atmosphere. Thermally induced low pressure is associated with convergence in the lower and middle troposphere. This convergence is manifested largely through the powerful low level Somali jet, which originates over the Indian Ocean in the Southern Hemisphere, traverses the Arabian Sea, crosses the west coast of India and the subcontinent, and curves cyclonically toward the foothills of the Tibetan Plateau. The air ascends partly through orographic lifting and partly through radiative and latent heating. It then turns south in the upper troposphere and returns to the Southern Hemisphere [*Johnson and Houze*, 1987].

The low level convergence is of course accompanied by compensating divergence aloft. This divergence is associated with a broad, strong anticyclonic circulation over the plateau, near the 200-mbar level. The warm air over the plateau actually produces a northward increase of midtropospheric temperature over India, and this temperature gradient is associated with strong upper level easterlies through the thermal wind relationship [*Murakami*, 1987; *Yanai et al.*, 1992; *Yanai and Li*, 1993]. The convectively active region associated with the Asian summer monsoon is particularly far north. Theoretical studies [e.g., *Hack et al.*, 1989] have shown that when the Intertropical Convergence Zone (ITCZ) migrates well to the north of the equator, the northern Hadley cell weakens, while the southern cell strengthens. In addition, conservation of angular momentum ensures that a northward migration of the ITCZ is associated with both low level westerlies and upper level easterlies, between the equator and the ITCZ [*Schubert et al.*, 1991].

Zhang [1994] investigated the sensitivity of the simulated Asian summer monsoon to the parameterization of cumulus convection in the atmospheric general circulation model (GCM) of the Canadian Climate Centre. He compared the results of a simulation with a mass flux–based convection parameterization using a buoyancy closure to results obtained with no convective parameterization at all and also to the results of a third simulation using moist convective adjustment. He found that in the simulations with moist convective adjustment and with no convection parameterization at all, the westerlies of the Somali jet extended unrealistically across Southeast Asia and into the western Pacific. The mass flux scheme produced a more realistic Somali jet, confined to the west of about 90°E longitude. The mass flux scheme also gave a more realistic distribution of precipitation, with plentiful rainfall over India, and the rainfall maximum in the western Pacific displaced toward the south, near the equator, as observed. The other two simulations gave less precipitation over India and moved the western Pacific precipitation maximum northward, contrary to observations. Zhang interpreted his results in terms of changes in the gross moist stability associated with the introduction of the mass-flux scheme.

Slingo et al. [1988] analyzed the response of the GCM of the European Centre for Medium Range Weather Forecasts (ECMWF) to changes in the radiation and convection parameterizations. They found a strong sensitivity of the simulated Asian summer monsoon, and especially the monsoon onset, to these parameterized processes.

The purpose of this paper is to further investigate the dependence of the Asian summer monsoon on parameterized physical processes by examining the results from several versions of the Colorado State University (CSU) GCM. Section 2 describes the versions of the CSU GCM used in this paper, in particular introducing the land-surface parameterization, the prognostically closed cumulus parameterization, and the stratiform cloud microphysics parameterization. The experiments essentially document the response of the simulated Asian summer monsoon to the evolution of the GCM over the past 7 years. Section 3 presents the Asian summer monsoon clima-

Paper number 1999JD900168.
0148-0227/99/1999JD900168$09.00

Table 1. Summary of Runs

Name of Run	Description of Run	Comments
Baseline	land surface: bucket model stratiform clouds: large-scale saturation value of α: 10^7 m^4 kg^{-1}	older, simpler version of the model
S2E	land surface: SiB2 stratiform clouds: Eauliq value of α: 10^7 m^4 kg^{-1}	newer, more complex version of the model
High-α	land surface: SiB2 stratiform clouds: Eauliq value of α: 10^9 m^4 kg^{-1}	Increasing α, relative to the baseline run, cools and moistens the atmosphere, as discussed by *Pan and Randall* [1998]

tology as simulated by the various versions of the GCM and compares these simulations with the observed climatology. Section 4 gives our conclusions. For an extended discussion of the topics covered in this paper, see *Eitzen* [1996].

2. Computational Design

2.1. Model Formulation

Each version of the CSU GCM to be examined in this paper has a fairly coarse horizontal grid spacing of 4° in the meridional and 5° in the zonal direction, which is adequate to represent the Indian peninsula but not fine enough to resolve the Western Ghats. The horizontal discretization is based on finite differences, following the methods of *Arakawa and Lamb* [1977, 1981]. The vertical structure of the atmosphere is represented using 17 layers, with a top at 51 mbar. The top two layers comprise the lower stratosphere, while the lowest layer is identically the planetary boundary layer (PBL). The PBL parameterization is described by *Suarez et al.* [1983]; it makes use of the assumption that the PBL is well-mixed in conservative variables. The PBL depth and the turbulence kinetic energy (TKE) are prognosed. All versions of the model as discussed in this paper use a modified *Arakawa and Schubert* [1974] cumulus parameterization [*Randall and Pan*, 1993; *Pan and Randall*, 1998], in which a prognostic cumulus kinetic energy is used in lieu of the strict quasi-equilibrium closure. The parameterizations of shortwave and longwave radiation follow the work of *Harshvardhan et al.* [1987, 1989].

The GCM has undergone rapid development over the past 5 years; we have replaced the cumulus parameterization [*Randall and Pan*, 1993; *Pan and Randall*, 1998; *Ding and Randall*, 1998], the land-surface parameterization [*Sellers et al.*, 1996a, b; *Randall et al.*, 1996], and the stratiform cloud parameterization [*Fowler et al.*, 1996; *Fowler and Randall*, 1996a, b]. These changes have led to major improvements in the simulation of the Asian summer monsoon, but because the changes were made in parallel and then merged, the current model expresses their combined effects.

For purposes of this paper, we define a "baseline" version of the model which uses the oldest versions of the model components under study. These include a "bucket model" land-surface parameterization [*Manabe*, 1969], a crude "large-scale saturation" parameterization of stratiform cloud processes, and a "low-α" version of the cumulus parameterization (explained below). In the course of the present study we analyzed the Asian summer monsoon simulations produced by this baseline version of the model. As discussed in detail below, the baseline run produces a rather poor simulation of the Asian summer monsoon.

The improved land-surface parameterization tested here is SiB2 [*Sellers et al.*, 1996a, b; *Randall et al.*, 1996], which takes into account the effects of vegetation on the surface fluxes of energy and water. Evaporation from the surface is regulated by vegetation in the SiB2 runs, whereas the baseline run (with the bucket model) determines the evapotranspiration solely on the potential evapotranspiration and the amount of moisture that is present relative to the field capacity. SiB2 includes two soil temperatures, as opposed to only one in the baseline; and SiB2 includes three soil moisture and two surface moisture stores, while the baseline version of the model only has a single ground wetness and no parameterization of surface wetness other than snow cover. Among the simulations analyzed in the course of our study is one in which the only change relative to the baseline run is the replacement of the bucket model by SiB2. The SiB2-only run is not discussed in section 3, however, because its results are similar to those of the baseline run; perhaps surprisingly, the improved land-surface parameterization did little to correct the deficiencies of the Asian summer monsoon as simulated by the baseline run. The surface air temperature field was modified by SiB2, but the wind and precipitation fields were almost unchanged. *Eitzen* [1996] gives a detailed analysis of the results of the SiB2-only run.

Eauliq [*Fowler et al.*, 1996; *Fowler and Randall*, 1996a, b] is a stratiform cloudiness parameterization which includes prognostic variables for cloud water, cloud ice, rain, and snow, as well as water vapor. It explicitly couples cumulus convection with stratiform anvils, includes such microphysical processes as the collection of cloud water by falling rain, and also includes a parameterization of the radiative properties of the clouds in terms of the predicted cloud water and cloud ice distributions. We performed a simulation which differs from the baseline run only through the replacement of the large-scale saturation parameterization by Eauliq. This Eauliq-only run is not discussed in this paper, however, because its results are similar to those of the S2E run (discussed below). *Eitzen* [1996] gives a detailed analysis of the results of the Eauliq-only run.

The S2E run listed in Table 1 differs from the baseline run through the addition of both SiB2 and Eauliq. As will be discussed in section 3, the results of the S2E run are considerably more realistic than those of the baseline run. The simulated precipitation distribution, in particular, is much improved over that of the baseline run.

We also examined the sensitivity of the simulated Asian summer monsoon to a simple but important change in the cumulus parameterization. The parameterization makes use of a prognostic cumulus kinetic energy, K, as discussed by *Randall and Pan* [1993] and *Pan and Randall* [1998]. The cumulus cloud base mass flux M_B is related to K by a parameter α:

$$M_B = \sqrt{K/\alpha}. \tag{1}$$

Table 2. Summary of Data Sources

Quantity	Data Source
850-mbar winds	ECMWF 1985–1988
200-mbar winds	ECMWF 1985–1988
Total precipitation rate	GPCC 1987–1995
500-mbar temperatures	ECMWF 1985–1988
Shortwave radiation absorbed at the surface	*Whitlock et al.* [1993]

Crudely speaking, $1/\alpha$ measures the efficiency with which convective available potential energy (CAPE) can be utilized to produce a cumulus mass flux. The mass flux warms and dries, tending to reduce the CAPE. When α is small, very little CAPE is needed to allow convective heating and drying, so the sounding tends to be warm and dry (corresponding to small values of the CAPE). When α is larger, more CAPE is needed to allow convective warming and drying, so the sounding tends to be cooler and more humid (corresponding to larger values of the CAPE). For a given value of K, larger α means smaller M_B. It is the value of M_B which actually determines the cumulus heating and drying rates, for a given thermodynamic sounding, so (1) implies that larger values of α reduce the cumulus heating and drying rates for a given value of K. As α is increased, the cumulus precipitation rate decreases and the stratiform precipitation rate increases [*Pan and Randall*, 1998]. In addition, larger values of α correspond to longer convective adjustment times, so that convective quasiequilibrium is enforced less rigidly. We emphasize that there is no reason whatsoever to suppose that α is a constant. We currently lack a theory to determine α, and so we assume constant values for simplicity, but we recognize the need to explore the sensitivity of our results to the value used. The baseline run uses $\alpha = 10^7$ m^4 kg^{-1}. We also performed a "high-α" run in which α was increased dramatically, by a factor of 100, to 10^9 m^4 kg^{-1}. The values of α considered here are compatible with the cumulus ensemble model results of *Xu and Arakawa* [1992]. The high-α run includes SiB2 and Eauliq, so we compare it with the S2E run. The effect of increasing α is to cool and moisten the atmosphere, leading a considerable improvement in the thermal structure and the associated thermal winds.

2.2. Data Sources

As noted earlier, the Asian summer monsoon can be thought of as a local Hadley circulation. To see if the model produces a realistic simulation of this circulation, we can break it up into three branches. The low level, northward branch of the circulation can be diagnosed using the winds at 850 mbar. The upward and downward branches can be diagnosed using precipitation. The upper level, southward branch can be diagnosed using the 200-mbar winds. The surface shortwave radiation is also examined.

We have compared our simulations with observations provided by the European Centre for Medium-Range Weather Forecasts (ECMWF) reanalysis project [*Gibson et al.*, 1996], the Surface Radiation Budget (SRB) satellite observations [*Whitlock et al.*, 1993] from NASA, and the precipitation data [*Xie and Arkin*, 1996] of the Global Precipitation Climatology Centre (GPCC). A "climatological" monsoon was simulated by using long-term average sea surface temperatures (SSTs) for the baseline run for a single January–December annual cycle. Observed 1985–1988 June–July–August (JJA) SSTs were used for all other runs. Table 2 lists the various observational data sets used in this study.

3. Results

Figure 1 shows the JJA-mean 850-mbar wind vectors from four years of ECMWF analyses averaged to 4° × 5° grid cells, and the results of the baseline run, the S2E run, and the high-α run. (For purposes of this paper the Asian monsoon region is defined to be bounded by (20°S, 30°E) and (40°N, 150°E). Figure 1 shows only this region.) The ECMWF 850-mbar wind analysis clearly shows the 15 m s^{-1} Somali jet that flows from the east coast of Africa, across the Arabian Sea, and onto the Indian subcontinent. The west coast of India and the west coast of Southeast Asia each experience strong onshore flow at 850 mbar from near the equator to about 20°N. Cross-equatorial flow occurs near the east coast of Africa. The equatorial flow is weak and nearly zonal east of 60°E, however. The ECMWF wind analyses could, in principle, be biased by the underlying model physics in regions with relatively few observations (such as over oceanic areas of the monsoon region.) However, the ECMWF winds were found to be consistent with other wind analyses [*van de Boogaard*, 1977; *Newell et al.*, 1972].

The baseline run produces a Somali jet, but it is stronger than observed, reaching a maximum speed (in the seasonal mean) of about 20 m s^{-1}. In the model, India and Southeast Asia experience onshore flow only south of about 15°N, and there is strong convergence over the southern portion of the Bay of Bengal. The simulated equatorial winds have a large meridional component for all longitudes shown and are much stronger than the observed winds in the same region. The baseline run also produced strong and unrealistic convergent westerly winds east of the Philippines. These unrealistic westerlies are similar to those obtained in some of the simulations discussed by *Zhang* [1994].

The S2E run also produces an excessively strong Somali jet, with winds of up to 20 m s^{-1}. The jet is in approximately the same position as that of the baseline run, with onshore flow over the west coasts of India and Southeast Asia from 0° to 15°N. The equatorial winds produced by the S2E run are much more realistic than those of the baseline run, however, in that they have only a small meridional component, except near the east coast of Africa. The winds to the east of the Philippines are also much more realistic than those of the baseline. As discussed below, these changes are associated with an Eauliq-induced reduction in the precipitation rate in the western Pacific, near 20°N, which was also reported by *Fowler et al.* [1996].

The Somali jet in the high-α run is weaker and more realistic than that of the S2E run. The westerly flow across central India is quite a bit stronger, and there is increased low level convergence over the northern Bay of Bengal. The winds to the east of the Philippines are similar to those simulated by the S2E run.

Figures 2 and 3 show the ECMWF-analyzed JJA 1985–1988 mean 200-mbar wind vectors and JJA 1985–1988 500-mbar temperatures, respectively, averaged to 4° × 5° grid cells. Figures 2 and 3 also show the results of the baseline run, the S2E run, and the high-α run. The ECMWF analysis shows 200-mbar easterlies ranging from 15 to 20 m s^{-1} over most of the monsoon region. The winds have a weak northerly component at the equator, especially in the eastern part of the monsoon region. The observed winds shift abruptly from easterlies to westerlies at the northern and southern fringes of the monsoon region, with westerlies of up to 30 m s^{-1} at about 35°N, which is where the poleward rate of change of temperature becomes strongly negative at 500 mbar. There is a broad anticyclonic circulation above most of the region at 25°N, which roughly cor-

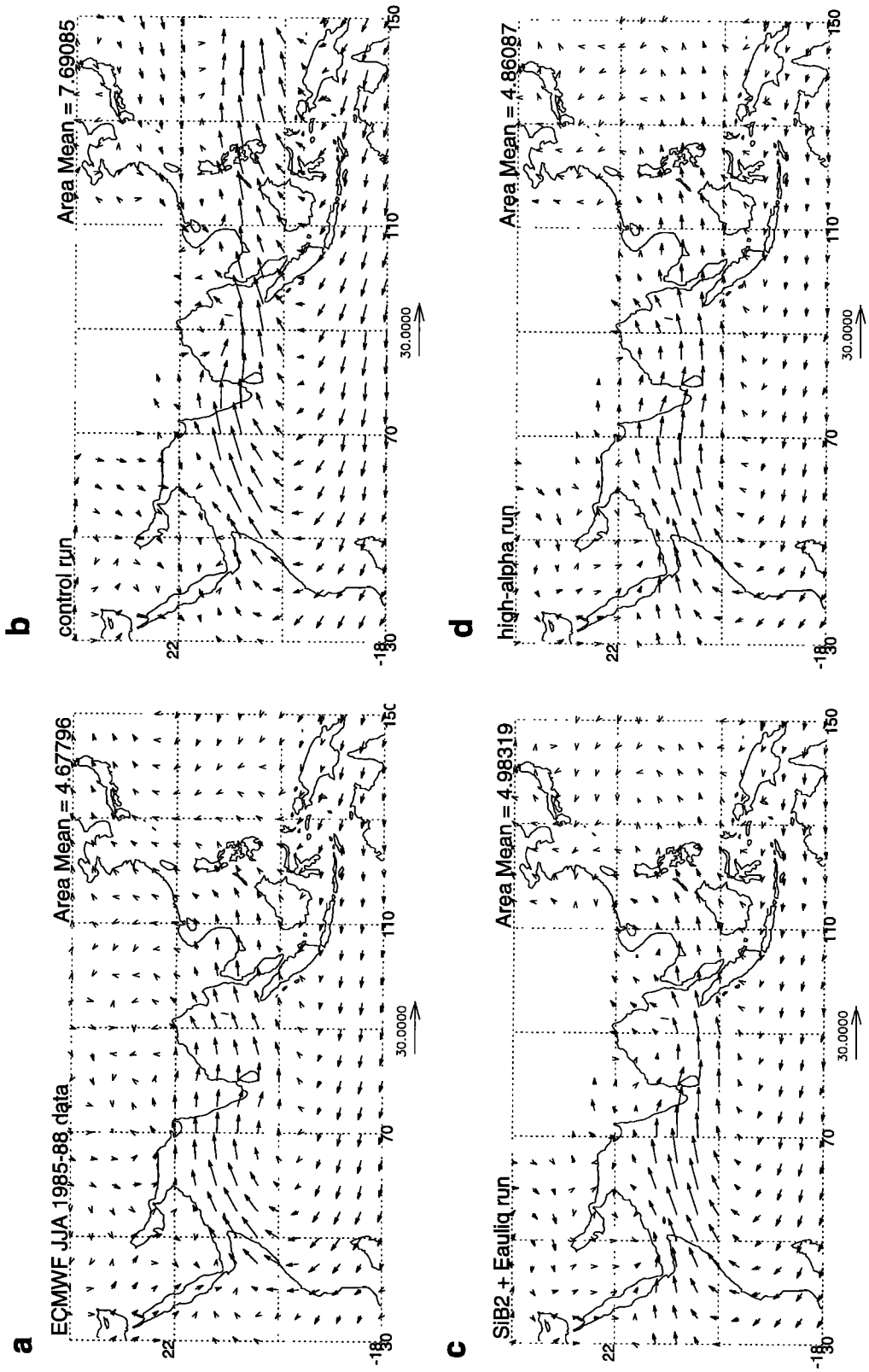

Figure 1. June–July–August (JJA) 850-mbar wind vectors for (a) ECMWF analyses averaged to 4° × 5° grid cells; (b) the baseline run; (c) the S2E run; and (d) the high-α run. A scale vector of 30 m s^{-1} is shown.

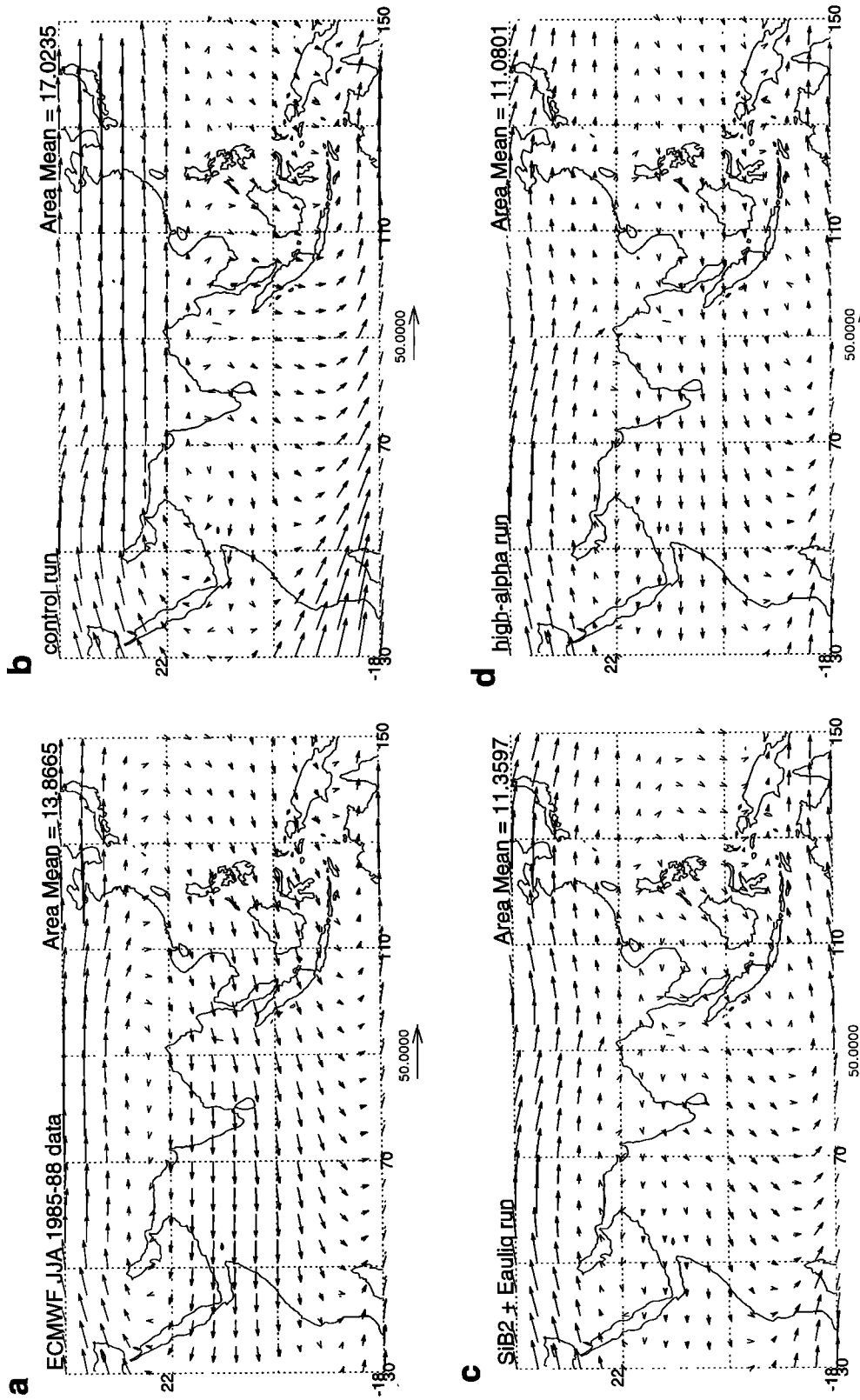

Figure 2. JJA 200-mbar wind vectors for (a) ECMWF analyses averaged to 4° × 5° grid cells; (b) the baseline run; (c) the S2E run; and (d) the high-α run. A scale vector of 50 m s^{-1} is shown.

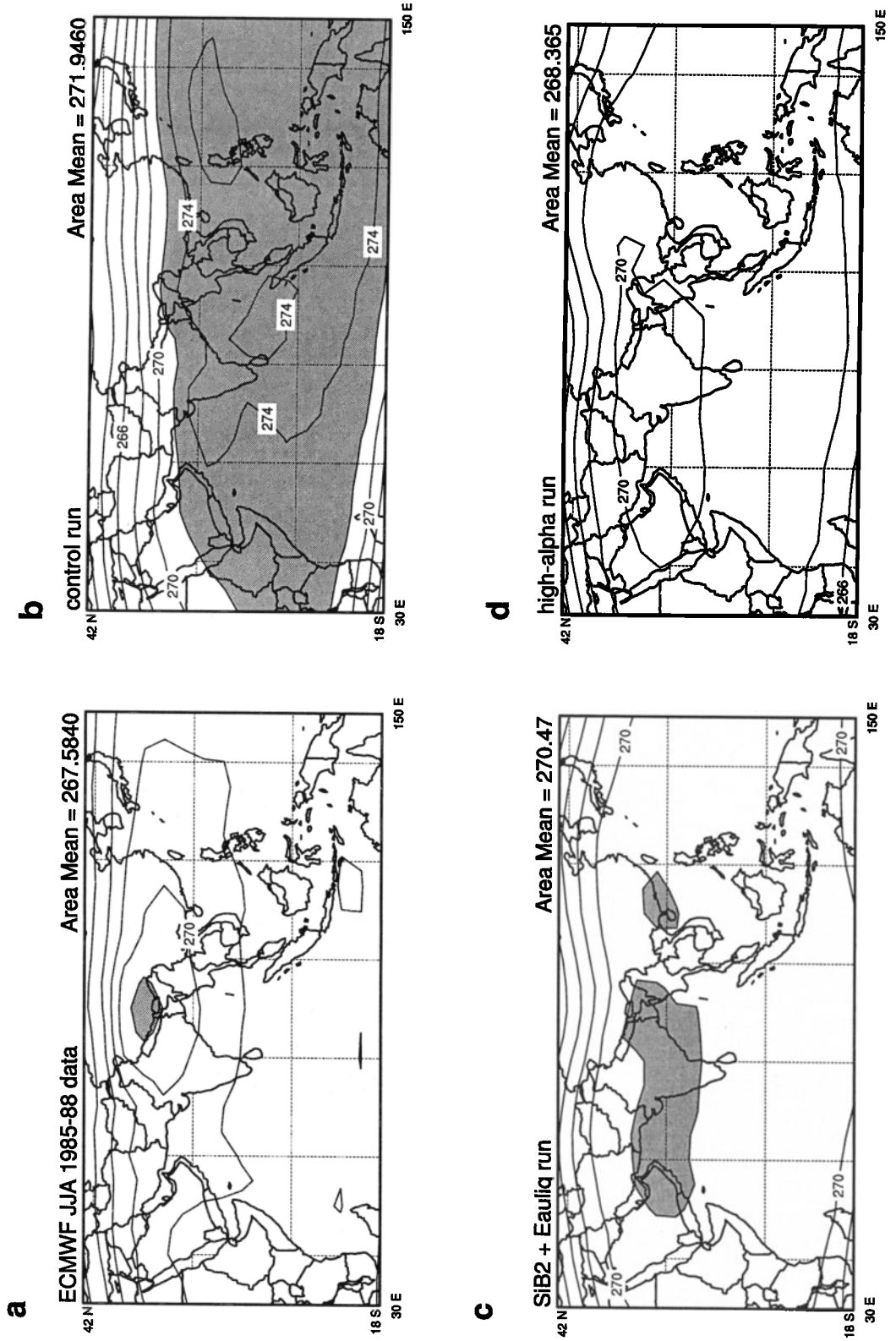

Figure 3. JJA 500-mbar temperatures for (a) ECMWF analyses averaged to 4° × 5° grid cells; (b) the baseline run; (c) the S2E run; and (d) the high-α run. The contour interval is 2 K. Values warmer than 272 K are shaded.

responds to a large area with temperatures in excess of 270 K. An island of warm temperatures can be seen over the Tibetan Plateau. The area-mean 500-mbar temperature is 268 K. The 500-mbar temperature field is quite flat overall, and the temperature range between the highest and lowest contours is only 8 K.

The baseline run produced very unrealistic 200-mbar winds and 500-mbar temperatures. There are almost no tropical easterlies at 200 mbar, and the simulated winds have a strong northerly component near the equator. In addition, the baseline run produced a huge area of temperatures warmer than 272 K between 20°N and 20°S, throughout the entire monsoon region. The winds at the northern and southern fringes of the monsoon region are similar to those observed, although somewhat stronger. This is consistent with the baseline run's stronger-than-observed meridional temperature gradient at 500 mbar over the same region. In contrast to the observations the baseline run does not produce an island of warm air over the Tibetan Plateau. The area-mean 500-mbar temperature is significantly higher than observed (272 K).

As shown in Figure 2c, the S2E run produced somewhat more realistic 200-mbar winds than did the baseline run. In the S2E run the simulated winds near the equator have an easterly component, particularly in the western part of the monsoon region. This is consistent with the results discussed by *Fowler and Randall* [1996a]. The simulated 200-mbar easterlies of the S2E run have a magnitude of only 5–10 m s^{-1}, however, which is much weaker than observed. The cross-equatorial flow in the eastern part of the monsoon region is stronger than observed but is nevertheless much weaker and more realistic than that of the baseline run. The S2E run also produced a more realistic simulation of the 500-mbar temperature than did the baseline run. The gradients are weaker, and correspondingly, the range of temperatures is reduced to only 8 K. The 272 K contour covers approximately the same region as the observed 270 K contour but does not enclose as large an area. The area-mean temperature is 271 K, which is still ~3 K warmer than observed. As in the baseline run, and unlike the observations, the S2E run fails to produce a clear temperature maximum over the Tibetan Plateau.

The 200-mbar easterlies produced by the high-α run are much stronger than those of the other runs, although still not quite as strong as observed. The Northern Hemisphere westerlies produced by the high-α run extend slightly farther south than observed, but not as far south as in the baseline run. The area-mean 500-mbar temperature simulated by the high-α run is about 2.1 K cooler than that simulated by the S2E run and is only about 1 K warmer than observed. The spatial pattern of the 500-mbar temperatures produced by the high-α run is similar to that observed, with a closed maximum over the Tibetan Plateau, although the simulated maximum is too wide in the zonal direction.

Another way to look at the winds and temperatures in the monsoon region is to plot the zonal wind and temperature as a function of latitude and pressure at a particular longitude which passes through the monsoon region. Figure 4 shows a latitude-pressure plot of the zonal wind and temperature at 77.5°E, based on ECMWF data that were first averaged onto the CSU GCM's grid. Figure 4 also includes similar plots of the results of the baseline, S2E, and high-α runs. Figure 5 is a similar plot, except that it shows the zonal wind and temperature fields of the baseline run subtracted from those of the S2E and high-α runs. The plots show that the baseline and S2E versions of the GCM do produce some easterlies in the monsoon region (between 20°S and 40°N), but they are both weaker and more limited in vertical extent than observed. The high-α run is much more successful at producing strong easterly winds, although they are higher and slightly weaker than observed. The observed thermal structure at 77.5°E is not realistic in the baseline run, but it is somewhat more realistic in both the S2E and high-α runs.

To gauge the effect of the different parameterizations on surface air temperature, Figures 6a and 6b show the surface air temperature field produced by the baseline run subtracted from the S2E and high-α runs, respectively. The increase in shortwave cloud forcing caused by the addition of Eauliq (as shown in Figure 7) has helped to produce decreases in the surface air temperature over most land areas except the Tibetan Plateau, which experiences a net increase in absorbed shortwave radiation and a slight increase in the surface air temperature.

In summary, the baseline simulation of the midtropospheric temperatures and upper tropospheric winds is very unrealistic. The introduction of Eauliq leads to significant improvements, but major problems still remain. The high-α run produces fairly realistic results.

Figure 8 shows JJA means of the precipitation across the monsoon region according to the GPCC data set, as averaged to 4° × 5° grid cells. It should be noted that precipitation is a difficult field to measure (particularly over the oceans), and there are significant differences among precipitation data sets. Also shown in Figure 8 are the corresponding results from the baseline run, the S2E run, and the high-α run. The observations show two major precipitation maxima: one west of the southwest coast of India and the other west of southern Burma. Both of these areas receive strong onshore flow. A minimum occurs near Sri Lanka, which appears to be affected by a lee-side rain shadow effect. The northern and western parts of the monsoon region are quite dry, receiving 2 mm d^{-1} of rain. The ECMWF 850-mbar wind analysis shows that these areas do not receive much moisture from the Indian Ocean during JJA. None of the monsoon region is observed to receive more than 20 mm d^{-1} of precipitation, and the area mean is ~4.2 mm d^{-1}.

The baseline run shows a large area with >20 mm d^{-1} of precipitation just north of the equator. There is a maximum west of the southwest coast of India, but it is stronger and farther to the west than the corresponding maximum in the GPCC data. The baseline run also produced maxima to the west of southern Burma and to the east of the Philippines, but these are again stronger than observed and coincide with regions of low level convergence over the Bay of Bengal and to the east of the Philippines that are higher than observed, as seen in the 850-mbar winds. The simulated mean precipitation rate is >50% higher than observed in the vicinity of the observed precipitation maxima, and the area-mean precipitation rate of ~6.0 mm d^{-1} is significantly higher than observed. At the same time, however, the baseline run produces less precipitation than observed over most of India.

The pattern of precipitation produced by the S2E run is somewhat more realistic than that of the baseline run. The precipitation maxima on the Arabian Sea and the Bay of Bengal are farther south than observed, but their magnitudes are more realistic than in the baseline run. The spurious and very strong precipitation maximum east of the Philippines, produced by the baseline run, is absent in the S2E run. This dramatic reduction in the simulated precipitation rate east of

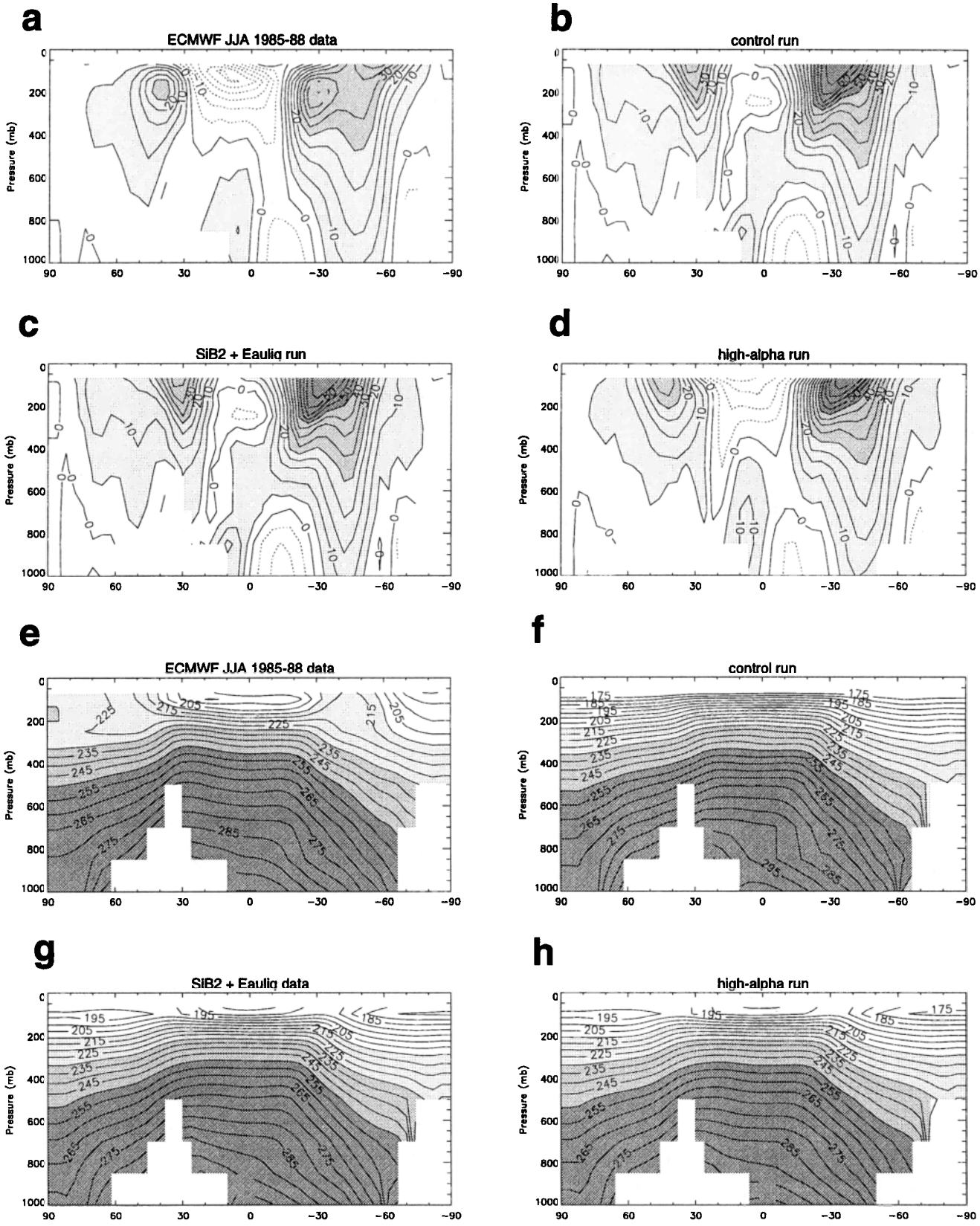

Figure 4. Latitude-pressure zonal wind plots at 77.5° E for (a) ECMWF analyses averaged to 4° × 5° grid cells; (b) the baseline run; (c) the S2E run; and (d) the high-α run. The contour interval is 5 m s^{-1}, and easterlies are dashed. The winds are not plotted below the surface of the Earth; we use the CSU model's orography to mask out "below-ground" values. (e)–(h) The corresponding results for the temperature, with a contour interval of 5 K.

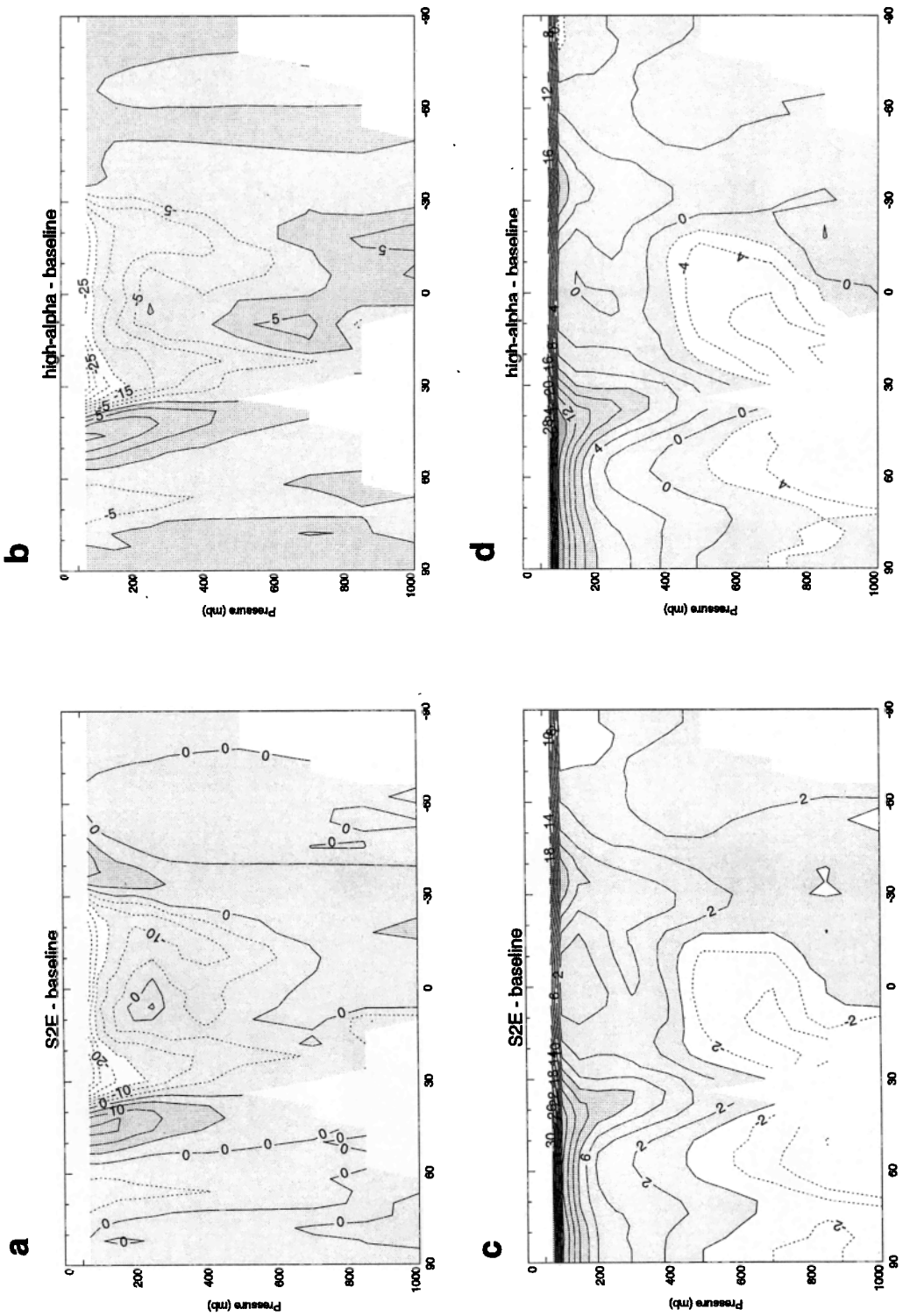

Figure 5. Latitude-pressure zonal wind plots at 77.5°E for baseline run subtracted from (a) the S2E run and (b) the high-α run. The contour interval is 5 m s^{-1}, and easterly differences are dashed. (c) and (d) The corresponding results for the temperature, with a contour interval of 2 K.

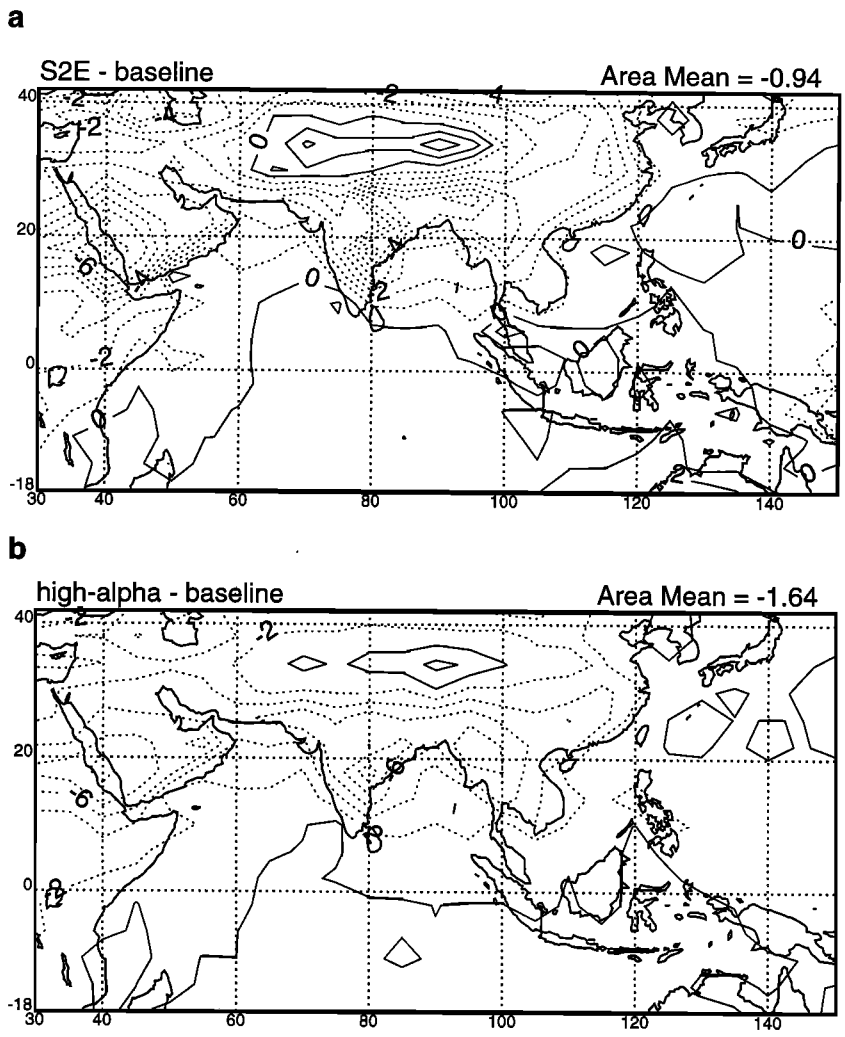

Figure 6. JJA surface air temperature field produced by the baseline run subtracted from those of the (a) S2E and (b) high-α runs. The contour interval is 1 K.

the Philippines, which was also reported by *Fowler et al.* [1996], appears to be responsible for the reduced eastward extension of the 850-mbar westerly jet, noted above. The reduction of the area-averaged precipitation rate to 5.5 mm d^{-1} is consistent with the global results of *Fowler et al.* [1996], who found that Eauliq produced significantly lower precipitation (particularly cumulus precipitation) than the large-scale saturation model. The reason is that Eauliq reduces the overall rate of global

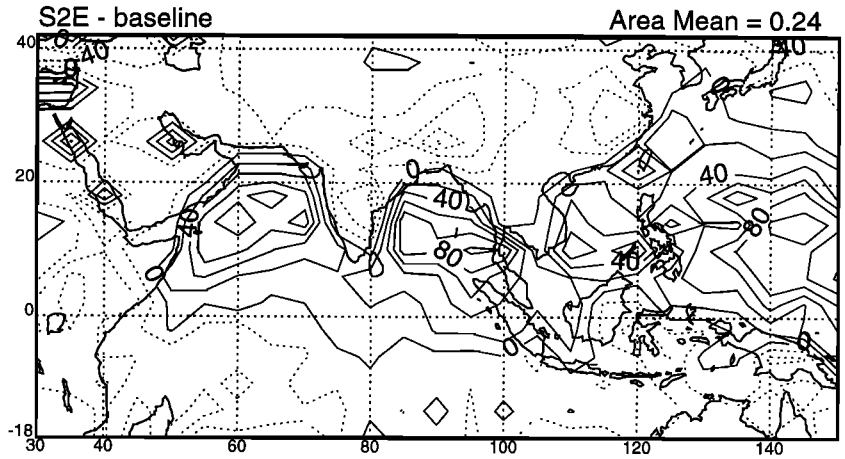

Figure 7. JJA surface shortwave cloud forcing difference for the baseline run subtracted from the S2E run. The contour interval is 20 W m^{-2}.

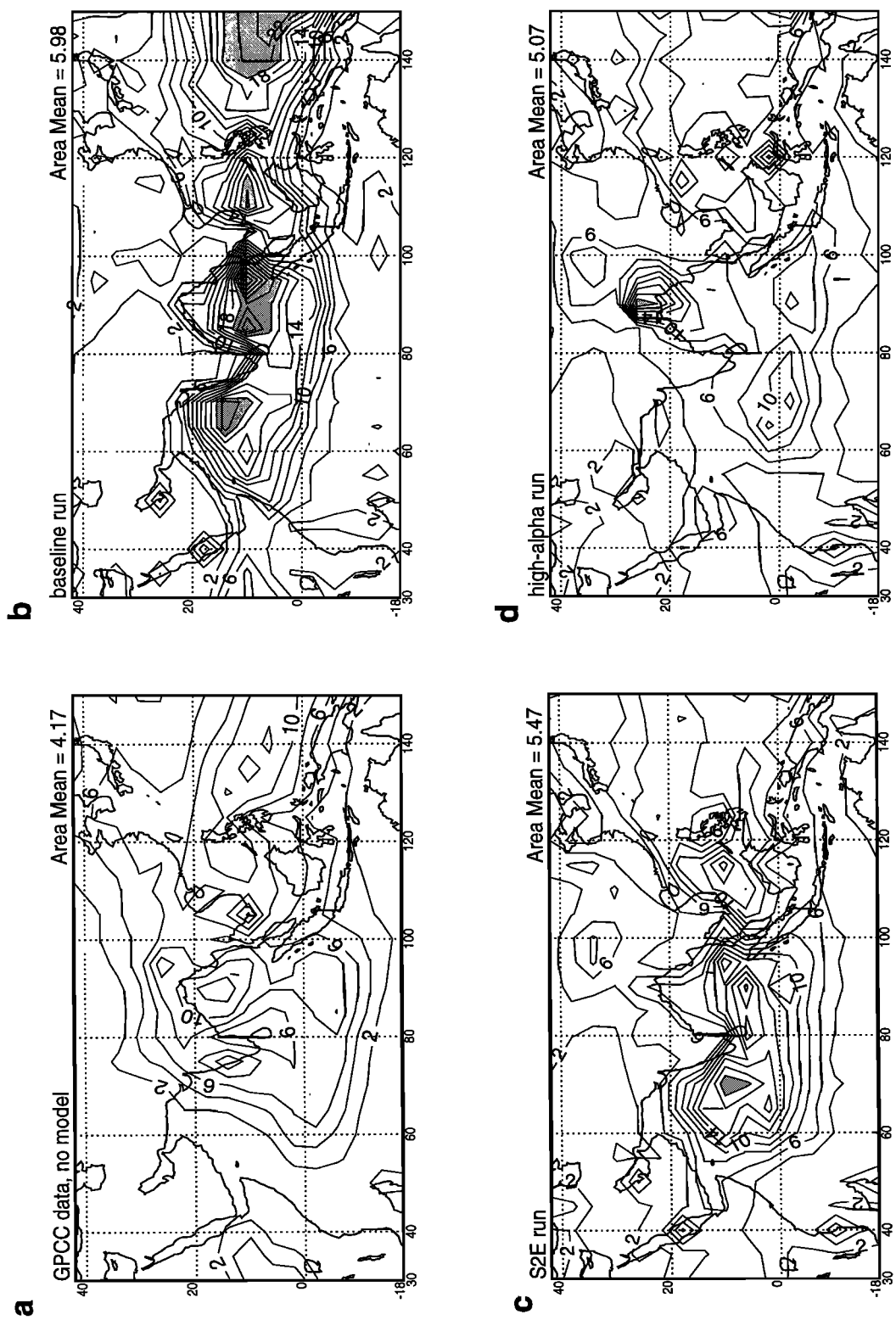

Figure 8. JJA precipitation in the monsoon region for (a) GPCC observations without model input averaged to 4° × 5° grid cells; (b) the baseline run; (c) the S2E run; and (d) the high-α run. The contour interval is 2 mm d^{-1}. Values higher than 20 mm d^{-1} are shaded.

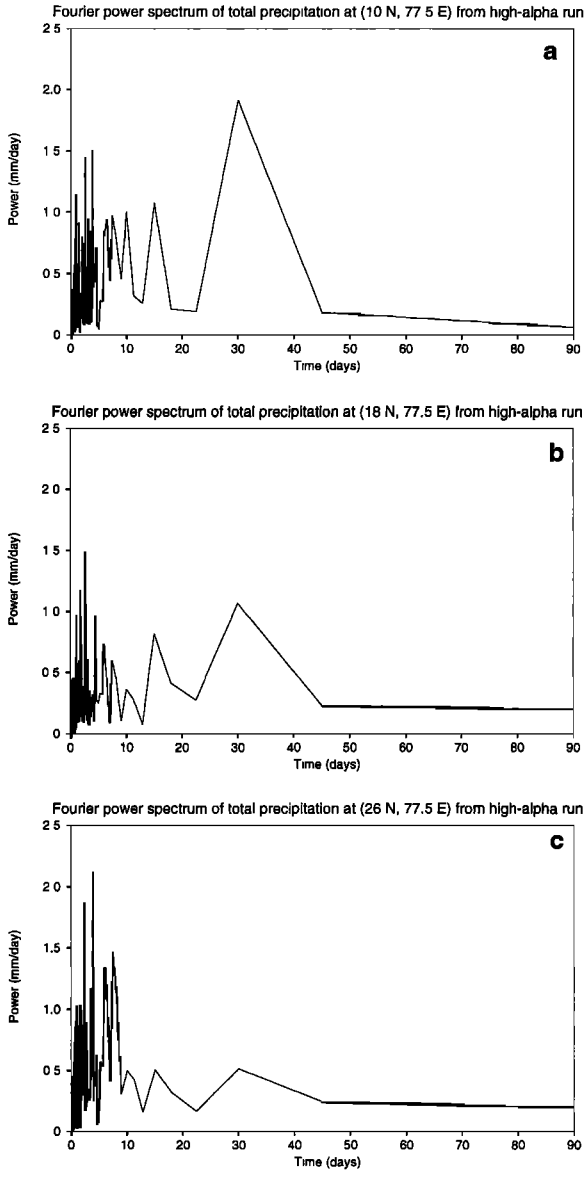

Figure 9. Temporal spectra of the simulated precipitation in the high-α run, based on hourly model output, for grid points at longitude 77.5°E, and at latitudes (a) 10°N, near the southern tip of India, (b) 18°N in central India, and (c) 26°N in northern India.

atmospheric radiative cooling; a corresponding reduction in precipitation is required for global energy balance.

The precipitation field produced by the high-α run is very different from that of the S2E run. The high-α run produced much less precipitation over most of the Arabian Sea and the southern Bay of Bengal. In contrast, the northern portions of the Bay of Bengal and Bangladesh receive much more precipitation. It appears that the observed Arabian Sea and Bay of Bengal precipitation maxima have been displaced to the south and north, respectively, in the high-α run. The area mean precipitation is lower than that of the S2E run, at 5.1 mm d^{-1}.

Webster [1987] has shown that intraseasonal monsoon precipitation varies on timescales of a few days owing to synoptic weather systems and 10–20 days owing to "breaks" in the monsoon. The S2E and high-α runs produce variations in precipitation on both of these timescales. Figure 9 shows the simulated temporal spectra of precipitation from the high-α run, for 77.5°E longitude, and for latitudes 10°N near the southern tip of India, 18°N in central India, and 26°N in northern India. The signal weakens toward the north. The simulated sea level pressure also exhibits variability on the same timescales (not shown).

Figure 10 shows the observed [*Randel et al.*, 1996] and simulated distributions of the precipitable water. The baseline run is much too dry, and the S2E run is slightly more moist. The high-α run is still slightly too dry but gives by far the most realistic simulation, including a realistic depiction of the observed precipitable water maxima in the Bay of Bengal and tropical western Pacific. This increase in precipitable water is consistent with the moistening and cooling of the atmosphere expected with an increase in α, as outlined in section 2.

The amount of shortwave radiation absorbed at the surface depends on the incident solar radiation at the top of the atmosphere, the shortwave cloud radiative forcing, gaseous absorption, and the surface albedo. The clouds of the summer monsoon reduce the shortwave radiation absorbed at the surface in the monsoon region. The observed [*Whitlock et al.*, 1993] JJA 1985–1988 mean surface net shortwave radiation for the monsoon region is shown in Figure 11. Also shown are the corresponding results from the baseline run, the S2E run, and the high-α run. The observed surface shortwave radiation is nearly uniform across the domain. The strongest minimum is centered over India, in a region that receives copious precipitation. There are many differences between the shortwave radiation field produced by the baseline run and the observed estimate. The baseline run produces a large area of high (>280 W m^{-2}) net shortwave radiation over a region stretching from northern India to the Arabian peninsula. The minimum net shortwave radiation occurs just north of the equator from the southern tip of India to the ocean east of Indonesia; this is the same region that receives the highest amount of precipitation in the baseline run. The S2E run produced a more realistic surface net shortwave radiation field. The area mean of 211 W m^{-2} is well below the observed mean, however. There are maxima in the northwest corner of the monsoon region in both the S2E run and the observations, although the observed maximum near the eastern edge of the region is not reproduced in the S2E run. The surface-absorbed shortwave radiation produced by the high-α run is similar to that of the S2E run. The highest values simulated by the high-α run are in the northwest portion of the monsoon region, as seen in both the S2E run and observations. The high-α run produced a strong minimum in surface net shortwave radiation northeast of the Bay of Bengal, which is to the east of and stronger than the observed minimum. Overall, the simulated amount shortwave radiation absorbed at the surface is much lower than observed.

4. Conclusions

In this paper we have compared simulations of the Asian summer monsoon with three versions of the CSU GCM. The baseline run gave a very poor simulation of the monsoon. Perhaps the greatest weakness of the baseline run was the glaring lack of a 200-mbar easterly flow over the monsoon region. The model did produce weak easterlies, but they were more limited in vertical extent than the observed easterlies.

Surprisingly, the improved land-surface parameterization had little effect on the simulated monsoon; the main impacts came from the improved stratiform cloud and convection pa-

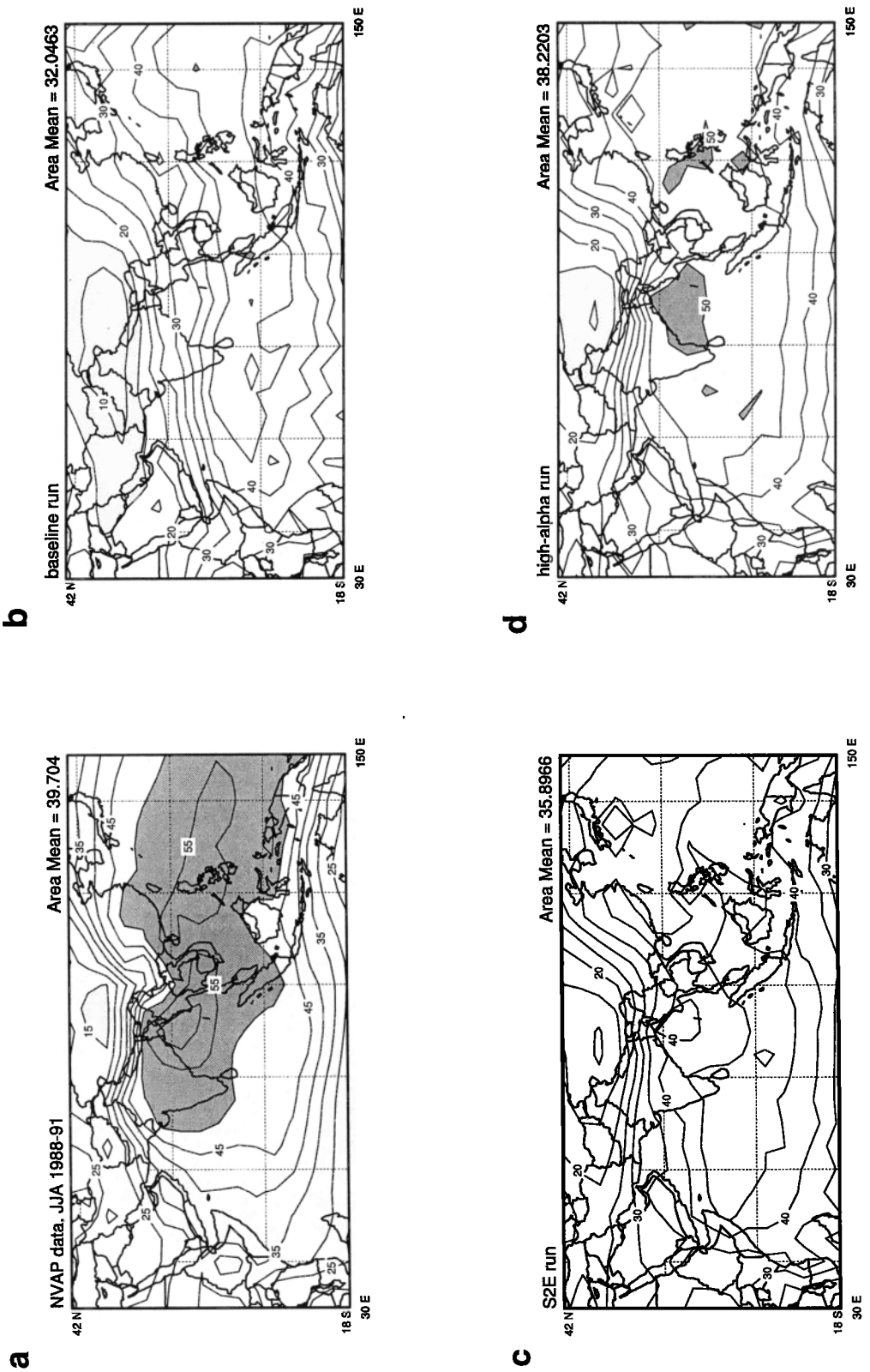

Figure 10. Precipitable water for (a) the observations of *Randel et al.* [1996] averaged to 4° × 5° grid cells; (b) the baseline run; (c) the S2E run; and (d) the high-α run. The contour interval is 2 mm. Light shading is used to denote values <15 mm, and dark shading is used for values >50 mm.

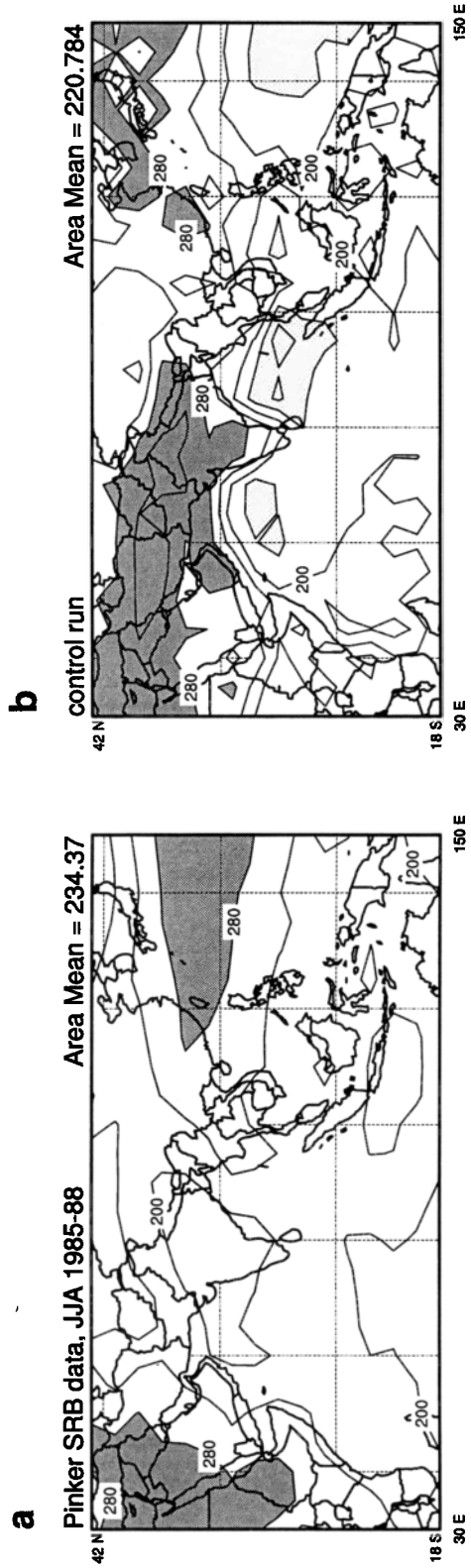

Figure 11. JJA net surface shortwave radiation for (a) the observations of *Whitlock et al.* [1993], averaged to 4° × 5° grid cells; (b) the baseline run; (c) the S2E run; and (d) the high-α run. The contour interval is 20 W m^{-2}. Light shading is used to denote values lower than 160 W m^{-2}, and dark shading is used for values higher than 280 W m^{-2}.

rameterizations. The introduction of Eauliq, the stratiform cloudiness parameterization developed by *Fowler et al.* [1996], leads to a reduced precipitation rate and a much more realistic geographical pattern of precipitation, which is accompanied by much more realistic lower tropospheric winds. Serious errors in the temperature field and the upper tropospheric wind field remain, however.

Perhaps the most dramatic result obtained in this paper is the substantial improvement in the realism of the simulated climate when a high value of α is used in our cumulus parameterization. As discussed earlier, increasing α makes the cumulus parameterization less effective in producing heating and drying; the sounding therefore becomes cooler, and the water vapor content of the atmosphere increases. The cooler, more humid sounding is considerably more realistic and permits a much more realistic upper tropospheric wind field as well.

Pan and Randall [1998] show that larger values of α correspond to longer convective adjustment times and looser quasi-equilibrium. Our results therefore suggest that convection parameterizations with finite convective adjustment times can give more realistic simulations of the summer monsoon circulation.

Acknowledgments. The authors thank the European Centre for Medium Range Weather Forecasts for the use of their analyses. This work was supported by the Department of Energy under grant DE-FG03-94ER61929 and by NSF under grant ATM-9214981. Computing resources were provided by NERSC at the Lawrence Berkeley Laboratory and by the Scientific Computing Division of the National Center for Atmospheric Research.

References

Arakawa, A., and V. R. Lamb, Computational design of the basic dynamical processes of the UCLA general circulation model, *Methods Comput. Phys.*, *17*, 173–265, 1977.

Arakawa, A., and V. R. Lamb, A potential enstrophy and energy conserving scheme for the shallow water equations, *Mon. Weather Rev.*, *109*, 18–36, 1981.

Arakawa, A., and W. H. Schubert, Interaction of a cumulus cloud ensemble with the large-scale environment, part I, *J. Atmos. Sci.*, *31*, 674–701, 1974.

Ding, P., and D. A. Randall, A cumulus parameterization with multiple cloud base levels, *J. Geophys. Res.*, *103*, 11,341–11,353, 1998.

Eitzen, Z. A., The simulation of the Asian summer monsoon by a general circulation model, M. S. thesis, Colo. State Univ., Fort Collins, 1996.

Fowler, L. D., and D. A. Randall, Liquid and ice cloud microphysics in the CSU general circulation model, 2, Simulation of the Earth's radiation budget, *J. Clim.*, *9*, 530–560, 1996a.

Fowler, L. D., and D. A. Randall, Liquid and ice cloud microphysics in the CSU general circulation model, 3, Sensitivity tests, *J. Clim.*, *9*, 561–586, 1996b.

Fowler, L. D., D. A. Randall, and S. A. Rutledge, Liquid and ice cloud microphysics in the CSU general circulation model, 1, Model description and simulated microphysical processes, *J. Clim.*, *9*, 489–529, 1996.

Gibson, R., P. Kallberg, and S. Uppala, The ECMWF re-analysis (ERA) project, *ECMWF Newsl.*, *73*, 7–17, 1996.

Hack, J. J., W. H. Schubert, D. E. Stevens, and H.-C. Kuo, Response of the Hadley circulation to convective forcing in the ITCZ, *J. Atmos. Sci.*, *46*, 2957–2973, 1989.

Harshvardhan, R. Davies, D. A. Randall, and T. G. Corsetti, A fast radiation parameterization for atmospheric general circulation models, *J. Geophys. Res.*, *92*, 1009–1016, 1987.

Harshvardhan, D. A. Randall, T. G. Corsetti, and D. A. Dazlich, Earth Radiation Budget and cloudiness simulations with a general circulation model, *J. Atmos. Sci.*, *46*, 1922–1942, 1989.

Johnson, R. H., and R. A. Houze Jr., Precipitating cloud systems of the Asian monsoon, in *Monsoon Meteorology*, edited by C.-P. Chang and T. N. Krishnamurti, pp. 298–353, Oxford Univ. Press, New York, 1987.

Legates, D. R., and C. J. Willmott, Mean seasonal and spatial variability in gauge-corrected global precipitation, *Int. J. Climatol.*, *10*, 111–127, 1990.

Manabe, S., Climate and ocean circulation, I, The atmospheric circulation and the hydrology of the Earth's surface, *Mon. Weather Rev.*, *97*, 739–774, 1969.

Murakami, T., Effects of the Tibetan Plateau, in *Monsoon Meteorology*, edited by C. P. Chang and T. N. Krishnamurti, pp. 235–270, Oxford Univ. Press, New York, 1987.

Newell, R. E., J. W. Kidson, D. G. Vincent, and G. J. Boer, *The General Circulation of the Tropical Atmosphere*, vol. 1, MIT Press, Cambridge, Mass., 1972.

Pan, D.-M., and D. A. Randall, A cumulus parameterization with a prognostic closure. *Q. J. R. Meteorol. Soc.*, *124*, 949–981, 1998.

Randall, D. A., and D.-M. Pan, Implementation of the Arakawa-Schubert cumulus parameterization with a prognostic closure, in *The Representation of Cumulus Convection in Numerical Models*, *Meteorol. Monogr. Ser.*, vol. 24, edited by K. Emanuel and D. Raymond, pp. 137–144, Am. Meteorol. Soc., Boston, Mass., 1993.

Randall, D. A., Harshvardhan, D. A. Dazlich, and T. G. Corsetti, Interactions among radiation, convection, and large-scale dynamics in a general circulation model, *J. Atmos. Sci.*, *46*, 1943–1970, 1989.

Randall, D. A., et al., A revised land-surface parameterization (SiB2) atmospheric GCMs, 3, The greening of the CSU general circulation model, *J. Clim.*, *9*, 738–763, 1996.

Randel, D. L., T. H. Vonder Haar, M. A. Ringerud, G. L. Stephens, T. J. Greenwald, and C. L. Combs, A new global water vapor dataset, *Bull. Am. Meteorol. Soc.*, *77*, 1233–1246, 1996.

Schubert, W. H., P. E. Ciesielski, D. E. Stevens, and H.-C. Kuo, Potential vorticity modeling of the ITCZ and the Hadley circulation, *J. Atmos. Sci.*, *48*, 1493–1509, 1991.

Sellers, P. J., D. A. Randall, G. J. Collatz, J. Berry, C. Field, D. A. Dazlich, C. Zhang, and L. Bounoua, A revised land-surface parameterization (SiB2) for atmospheric GCMs, 1, Model formulation, *J. Clim.*, *9*, 676–705, 1996a.

Sellers, P. J., S. O. Los, C. J. Tucker, C. O. Justice, D. A. Dazlich, G. J. Collatz, and D. A. Randall, A revised land-surface parameterization (SiB2) for atmospheric GCMs, 2, The generation of global fields of terrestrial biophysical parameters from satellite data, *J. Clim.*, *9*, 706–737, 1996b.

Slingo, J. M., U. C. Mohanty, M. Tiedtke, and R. P. Pearce, Prediction of the 1979 summer monsoon onset with modified parameterization schemes, *Mon. Weather Rev.*, *116*, 328–346, 1988.

Suarez, M. J., A. Arakawa, and D. A. Randall, The parameterization of the planetary boundary layer in the UCLA general circulation model: Formulation and results, *Mon. Weather Rev.*, *111*, 2224–2243, 1983.

van de Boogaard, H., The mean circulation of the tropical and subtropical atmosphere—July, *NCAR Tech. Note NCAR/TN-118+STR*, Natl. Cent. for Atmos. Res., Boulder, Colo., 1977.

Webster, P. J., The variable and interactive monsoon, in *Monsoons*, edited by J. S. Fein and P. L. Stephens, pp. 269–330, John Wiley, New York, 1987.

Whitlock, C. H., T. P. Charlock, W. F. Staylor, R. T. Pinker, I. Laszlo, R. C. DiPasquale, and N. A. Ritchey, WCRP surface radiation budget shortwave data product description—Version 1.1, *NASA Tech. Memo. TM-107747*, 1993.

Xie, P., and P. A. Arkin, Analyses of global monthly precipitation using gauge observations, satellite estimates, and numerical model predictions, *J. Clim.*, *9*, 840–858, 1996.

Xu, K.-M., and A. Arakawa, Semi-prognostic tests of the Arakawa-Schubert cumulus parameterization using simulated data, *J. Atmos. Sci.*, *49*, 2421–2436, 1992.

Yanai, M., and C. Li, Mechanism of heating and the boundary layer over the Tibetan Plateau, *Mon. Weather Rev.*, *122*, 305–323, 1993.

Yanai, M., C. Li, and Z. Song, Seasonal heating of the Tibetan Plateau and its effects on the Asian summer monsoon, *J. Meteorol. Soc. Jpn.*, *70*, 319–351, 1992.

Zhang, G. J., Effects of cumulus convection on the simulated monsoon circulation in a general circulation model, *Mon. Weather Rev.*, *122*, 2022–2038, 1994.

Z. A. Eitzen and D. A. Randall, Department of Atmospheric Science, Colorado State University, Fort Collins, CO 80525. (zach@cornice.atmos.colostate.edu)

(Received June 12, 1998; revised February 10, 1999; accepted February 25, 1999.)